Physics and Chemistry of Minerals (2020) 47:21
https://doi.org/10.1007/s00269-020-01089-4

ORIGINAL PAPER

Phase transition of sanidine ($KAlSi_3O_8$) and its effect on electrical conductivity at pressures up to 11 GPa

Xinzhuan Guo[1,2] · Sibo Chen[3] · Ping Li[4] · Yanfei Zhang[5] · Xiang Wu[2] · Junfeng Zhang[2]

Received: 14 December 2019 / Accepted: 2 March 2020

Abstract

Sanidine is an important crustal mineral whose high-pressure phase, liebermannite, can be carried down to the mantle transition zone by the subducting slab. Owing to the characteristic channel structure of liebermannite, which can provide a pathway for K^+ along the [001] direction, it can serve as a highly conductive phase. In this study, we measured the electrical conductivity of natural sanidine at pressures of up to 11 GPa. The results show that electrical conductivity decreased during the phase transition of sanidine to a mixture of $K_2Si_4O_9$ wadeite, kyanite, and coesite at 8 GPa, and further to liebermannite at 11 GPa. Accordingly, the activation enthalpy increased from 1.24 to 1.39 eV, and further to 1.47 eV during the phase transitions. Polycrystalline liebermannite with a high concentration of K^+ vacancies (35%) did not exhibit highly conductive behavior when the lattice-preferred orientation was not developed. Compared with the theoretically calculated conductivity of liebermannite with a K^+ vacancy of 25% along the [001] direction, the single-crystal liebermannite was highly anisotropic (given simply by the difference between $\log\sigma_{max}$ and $\log\sigma_{min}$), at least higher than 4. Furthermore, the electrical conductivity of polycrystalline liebermannite was approximately one order of magnitude lower than that measured by geophysical observations (0.1 S/m) in the transition zone beneath Northeastern (NE) China and the Philippine Sea, and could not be used to interpret high-conductivity anomalies without a preferred orientation along the [001] direction.

Keywords Sanidine · Liebermannite · Electrical conductivity · Phase transition · Transition zone · High-conductivity anomalies

Introduction

Alkali feldspars with the composition (K, Na)$AlSi_3O_8$ are the most abundant minerals in the Earth's crust (Le Bas et al. 1986), and can be divided into two groups based on structure: monoclinic and triclinic symmetry. Sanidine, one end-member of potassium feldspar, belongs to the monoclinic group. Comparing to orthoclase, a monoclinic polymorph, and microcline, a triclinic polymorph, sanidine is stable at highest temperatures. Solid K–Na solutions always occur in this group. Because potassium feldspar can be carried down to the Earth's interior via the subduction process (Holmann 1997), phase equilibrium experiments on the composition of $KAlSi_3O_8$ under high temperature and pressure have been extensively conducted. The results have confirmed that sanidine first dissociates into a mixture of $K_2Si_4O_9$ wadeite, kyanite, and coesite at 6–7 GPa and recombines into liebermannite (K-hollandite) at 9–10 GPa (Chang et al. 2013; Urakawa et al. 1994; Yagi et al. 1994; Akaogi et al. 2004). Liebermannite transforms into liebermannite II, which is an unquenchable high-pressure phase at 20–23 GPa and temperatures of 300–1000 K (Nishiyama et al. 2005; Liu et al. 2006; Sueda et al. 2004). Liebermannite is the most abundant phase in continental crusts at pressure and temperature conditions corresponding to the transition

✉ Xinzhuan Guo
gxzhuan@mail.gyig.ac.cn

1 Key Laboratory for High-Temperature and High-Pressure Study of the Earth's Interior, Institute of Geochemistry, Chinese Academy of Sciences, Guiyang 550081, China

2 State Key Laboratory of Geological Processes and Mineral Resources, School of Earth Sciences, China University of Geosciences, Wuhan 430074, China

3 Department of Geosciences, Stony Brook University, Stony Brook, NY 11794-2100, USA

4 School of Ocean and Earth Science, Tongji University, Shanghai 200092, China

5 College of Oceanography, Hohai University, Nanjing 210098, China

Published online: 12 March 2020

zone (Irifune et al. 1994). It should be noted that natural occurrences of $KAlSi_3O_8$–hollandite were first discovered in a shocked basaltic meteorite by Langenhorst and Poirier (2000). Then, Ma et al. (2018) reported the occurrence of $KAlSi_3O_8$ in hollandite-type structure in the Martian shergottite Zagami and proposed the name of liebermannite for this new mineral (Chen et al. 2019).

Liebermannite, with a tetragonal hollandite-type structure, is composed of four double chains of edge-shared (Si, Al)O_6 octahedra that form a large, enclosed square channel along the [001] axis, with K occupying the sites in the channel. Liebermannite is a potential host for large ions of lithophile elements (LILEs) of geochemical importance that can be accommodated in the channel structure, and carried down into the mantle transition zone and the lower mantle (Ringwood et al. 1967; Yamada et al. 1984). The large channel structure of liebermannite likely provides a path for the migration of K^+. Some materials sharing the hollandite structure (e.g., hollandite-type $K_xTi_{1-y}Mn_yO_2$) show distinctively high conductivity (20 S/m) even at room temperature (Khanna et al. 1981). First-principle calibrations have shown that 6% of K^+ vacancies in liebermannite can lead to a higher conductivity than that of hydrated wadsleyite and ringwoodite in the mantle transition zone, and 25% of K^+ vacancies can lead to a conductivity higher than $10^{0.5}$ S/m along [001] at 1000 K and the depth of the transition zone (He et al. 2016). Therefore, it might contribute to high-conductivity anomalies in the transition zone beneath NE China and the Philippine Sea (He et al. 2016).

However, no experiments focusing on electrical conductivity have been conducted to investigate the electrical properties of liebermannite. In this study, we carried out experiments on the phase transition of $KAlSi_3O_8$ at high pressure ranging from 3 to 11 GPa and measured the electrical conductivity of sanidine at 3 GPa, a mixture of wadeite-type $K_2Si_4O_9$, kyanite, and coecite at 8 GPa, and liebermannite at 11 GPa. The electrical conductivity of polycrystalline liebermannite was found to be well below that predicted by theoretical calculations. As a result, polycrystalline liebermannite without a preferred orientation along the [001] direction cannot contribute to high-conductivity anomalies in the transition zone beneath NE China and the Philippine Sea.

Experimental methods

Natural sanidine was used as starting material for the electrical conductivity measurements. The pale red sample was fresh, free of any alteration. Microstructural observations of the sample by a field emission gun scanning electron microscope (FEG-SEM) showed that lamella-like albite intergrew with the sanidine (Fig. 1). The volume fraction of albite was around 10%. We also synthesized sanidine as the starting material, following the method developed by Urakawa et al. (1994), to confirm its phase transition to the mixture of wadeite-type $K_2Si_4O_9$, kyanite, and coecite at 8 GPa. The powdered mixture of K_2CO_3, Al_2O_3, and SiO_2 at the designed ratio was decarbonated at 1073 K for 3 h in a stove. This mixture was melted at 5 GPa and 1973 K for 15 min, and was crystallized at 1573 K for 10 h. These two starting materials were checked by Raman spectroscopy. The chemical compositions of natural and synthesized sanidine (Table 1) were determined using a JXA-8100 electron probe microanalyzer set at 15 kV and 20 nA with a 3-μm beam at the State Key Laboratory of Geological Processes and Mineral Resources of the China University of Geosciences (Wuhan). Natural sanidine contains a small amount of Na, and the albite inclusion is almost free of K. The chemical composition of the synthesized sample was close to its stoichiometry. The natural sanidine was cored to disks with a thickness of 0.5 mm and diameter of 1.5 mm using an ultrasonic drilling machine. It was then baked at 120 ℃ to eliminate the absorbed water before measuring electrical conductivity. The synthesized sanidine was milled into powder with a grain size of around 10 μm, and was then compressed into a disk with a thickness of 0.5 mm and diameter of 1.5 mm using a hand press.

High pressures and temperatures were generated using a Rockland 1000-ton walker-type multianvil apparatus installed at the China University of Geosciences (Wuhan), and eight tungsten carbide cubes with a truncation of 8 mm were used as second-stage anvils. A Cr_2O_3-doped MgO octahedron with edges of length of 14 mm was used as pressure medium. The cell assembly used for measuring electrical conductivity is shown in Fig. 2. A $LaCrO_3$ sleeve, an MgO tube, and molybdenum disks were used as the heater, the sample capsule, and the electrodes, respectively. Slim tubes of Al_2O_3 were used to insulate the thermocouples from the surrounding materials, and could efficiently protect the thermocouples under high pressure. The pressure calibration of this cell assembly has been determined elsewhere (Chen et al. 2018). To exclude absorbed water, all parts composed of MgO, Al_2O_3, or ZrO_2 were baked at 1273 K for longer than 1 h prior to the experiments.

To measure electrical conductivity, a Solartron 1260 impedance–gain–phase analyzer was used in combination with a Solartron 1296 dielectric interface to measure the resistance of the sample at high pressure and temperature, and was operated using a 1 V sinusoidal signal at frequencies ranging from 1 M to 0.1 Hz. We obtained the sample's resistance by fitting the impedance spectra using *Z*-view software. The electrical conductivity (σ) was calculated using $\sigma = \frac{l}{SR}$, where l is the length of the sample, S is its cross-sectional area, and R is its resistance. We sequentially measured the electrical conductivity of the

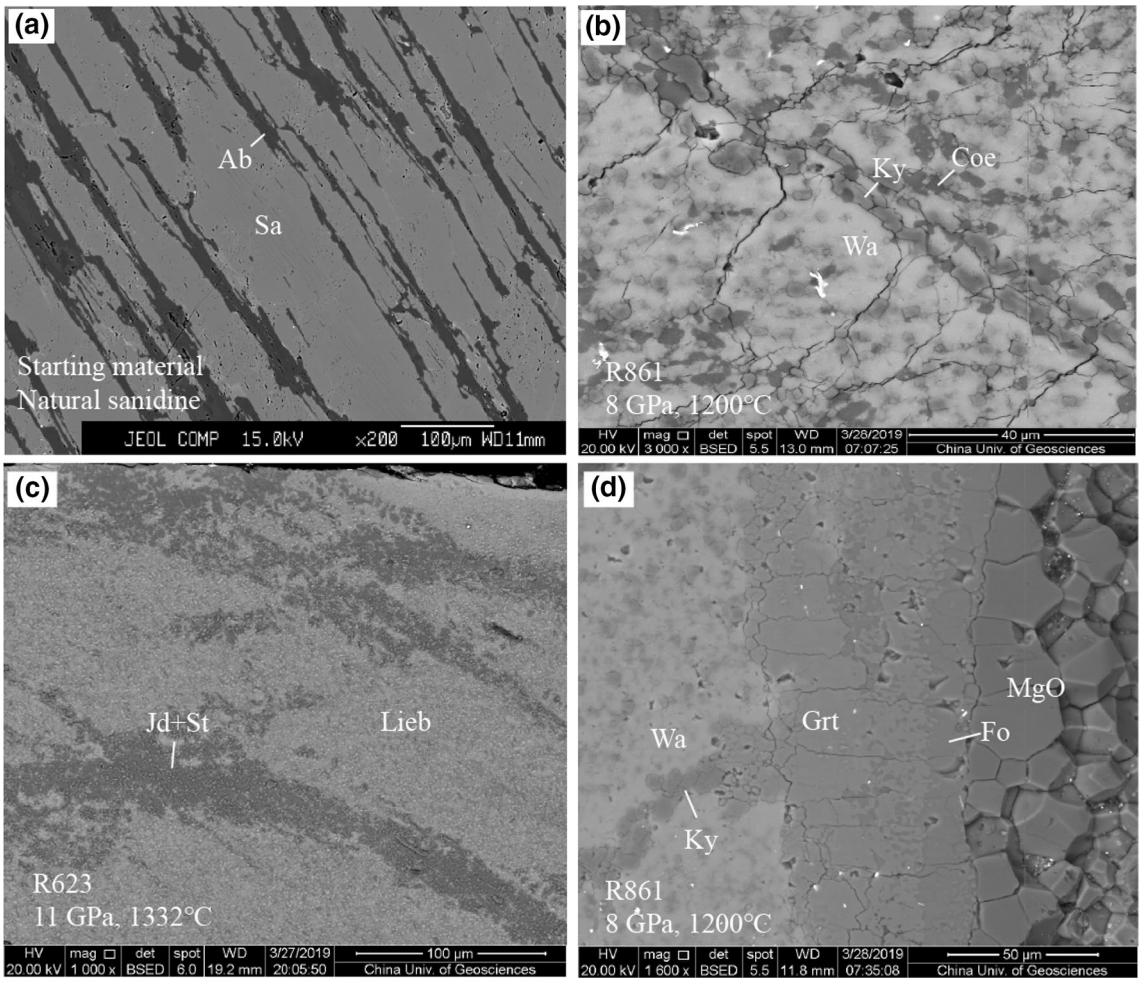

Fig. 1 Back-scattered images of the starting material and recovered samples. **a** Albite lamella (10 vol.%) coexists with sanidine in the starting material. **b** Recovered sample of R861. The coexisting assemblage is $K_2Si_4O_9$–wadeite, kyanite, and coesite. **c** Recovered sample of R623. The coexisting phases consisted of liebermannite, jadeite, and stishovite. **d** Two reaction rims were observed between the sample and the MgO capsule for the recovered sample of R861. *Ab* albite, *Sa* sanidine, *Ky* kyanite, *Co* coesite, *Jd* jadeite, *St* stishovite, *Lieb* liebermannite, *Grt* garnet

sample at 3 GPa and 1000–1500 K, that of a mixture of wadeite-type $K_2Si_4O_9$, kyanite, and coecite at 8 GPa and 1000–1600 K, and that of liebermannite at 11 GPa and 1000–1600 K. Complex impedance spectra were acquired at intervals of 100 K in the heating path and 50 K in the cooling path.

Following conductivity measurements, the textures of the recovered samples were analyzed using FEG-SEM using both the secondary electron image (SEI) and the backscattered electron image (BEI). Phases of the products of different runs were confirmed using a micro-focused laser Raman Spectroscopy (Fig. 3). The chemical composition of each phase was analyzed using electron microprobe analysis (Table 1).

Results and discussion

The representative impedance spectra of the sample are shown in Fig. 4. Impedance is a complex quantity that includes ohmic resistance (the real component) and reactance (the imaginary component). An equivalent circuit consisting of a resistance (R) and a constant phase element (CPE) in parallel was used to fit the experimental data with the results of the Z-view software to obtain the sample's resistance (fitting error within 5%). Measurements of the impedance spectra show that the sample's resistance was strongly dependent on temperature and pressure. The resistance decreased with increasing

Table 1 Chemical composition of the starting materials and the run products

	Sa ($n=5$)	Ab ($n=2$)	Jd ($n=7$)	K-Hol ($n=6$)
SiO_2	63.74	66.93	64.63	68.23
TiO_2	0.00	0.01	0.01	0.00
Al_2O_3	18.02	19.14	23.07	17.68
$FeO^{\dagger}$	0.15	0.17	0.37	0.13
MnO	0.01	0.00	0.013	0.00
MgO	0.00	0.01	0.028	0.01
CaO	0.00	0.21	0.826	0.04
Na_2O	1.19	11.27	10.57	1.28
K_2O	14.76	0.15	0.52	9.18
Cr_2O_3	0.00	0.01	0.027	0.02
Total	97.88	97.90	100.00	96.57
O	8	8	6	8
Si	3.00	2.99	2.13	3.12
Ti	0.00	0.00	–	0.00
Al	1.00	1.01	0.90	0.95
Fe[a]	0.01	0.01	0.01	–
Mn	0.00	0.00	–	–
Mg	0.00	0.00	–	–
Ca	0.00	0.01	0.03	–
Na	0.11	0.98	0.68	0.11
K	0.89	0.01	0.02	0.54
Cr	0.00	0.00	–	0.00
Total	5.00	5.00	3.77	4.73

[a]Assuming all Fe as FeO

n is the total number of the analyzed points

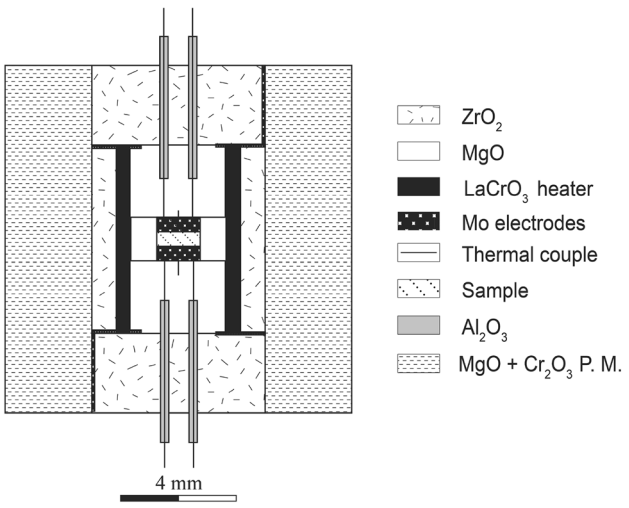

Fig. 2 Schematic cross-section of cell assembly for electrical conductivity measurements

temperature and increased with increasing pressure. Its temperature dependence indicates that phases measured in each condition exhibited semi-conductor-like behavior.

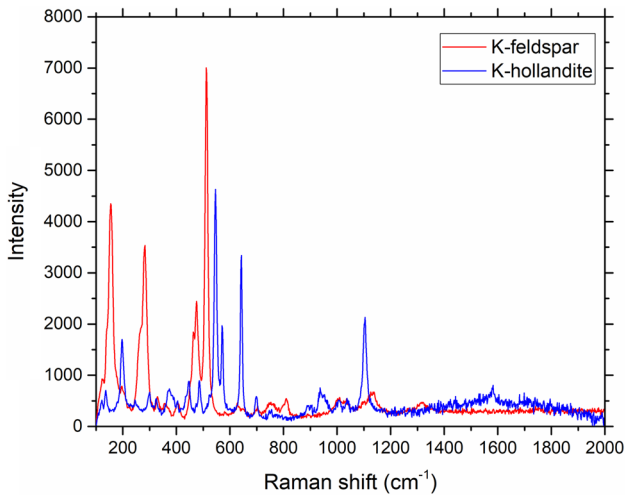

Fig. 3 Raman spectra of the starting material of K-feldspar (sanidine) and the run product of liebermannite (K-hollandite)

The pressure dependence was caused by the effect of the phase transition.

Figure 5 shows the relationship between electrical conductivity (σ) and temperature at 3, 8, and 11 GPa. At each pressure, the electrical conductivity–temperature relationship can be expressed by the Arrhenian formula:

$$\sigma = \sigma_0 \exp\left(-\frac{H}{kT}\right) \quad (1)$$

where σ_0 is a pre-exponential factor (S/m), H is activity enthalpy (eV), k is the Boltzmann constant (J/K), and T is absolute temperature (K). A single activation enthalpy could be defined in the investigated range of temperature. For R623, the activation enthalpy increased from 1.24 eV at 3 GPa to 1.39 eV at 8 GPa, and further to 1.47 eV at 11 GPa. The errors are derived from the estimation of sample's dimensions, temperature (±2 ℃), and the data fitting. After the experiments, we re-measured the sample's dimension and re-corrected the conductivity data. The total errors are less than 7% in conductivity. With pressure increasing from 3 to 8 GPa and then to 11 GPa, the electrical conductivity decreased in the same range of temperature. The phase transitions of sanidine to the mixture of wadeite-type $K_2Si_4O_9$, kyanite, and coecite at 8 GPa, and further to liebermannite at 11 GPa inhibited electrical conductivity. Liebermannite in particular did not exhibit highly conductive behavior. To check the quality of the data, an experiment on R643 was conducted. The conductivities of R643 were almost consistent with those of R623 at 3 GPa and 8 GPa. The conductivity of sanidine at 3 GPa was slightly higher than that reported by Hu et al. (2013), but lower than that of albite at 1 GPa (Guo et al. 2015). The electrical conductivity of a solid solution of alkali feldspar has been reported to increase with increasing

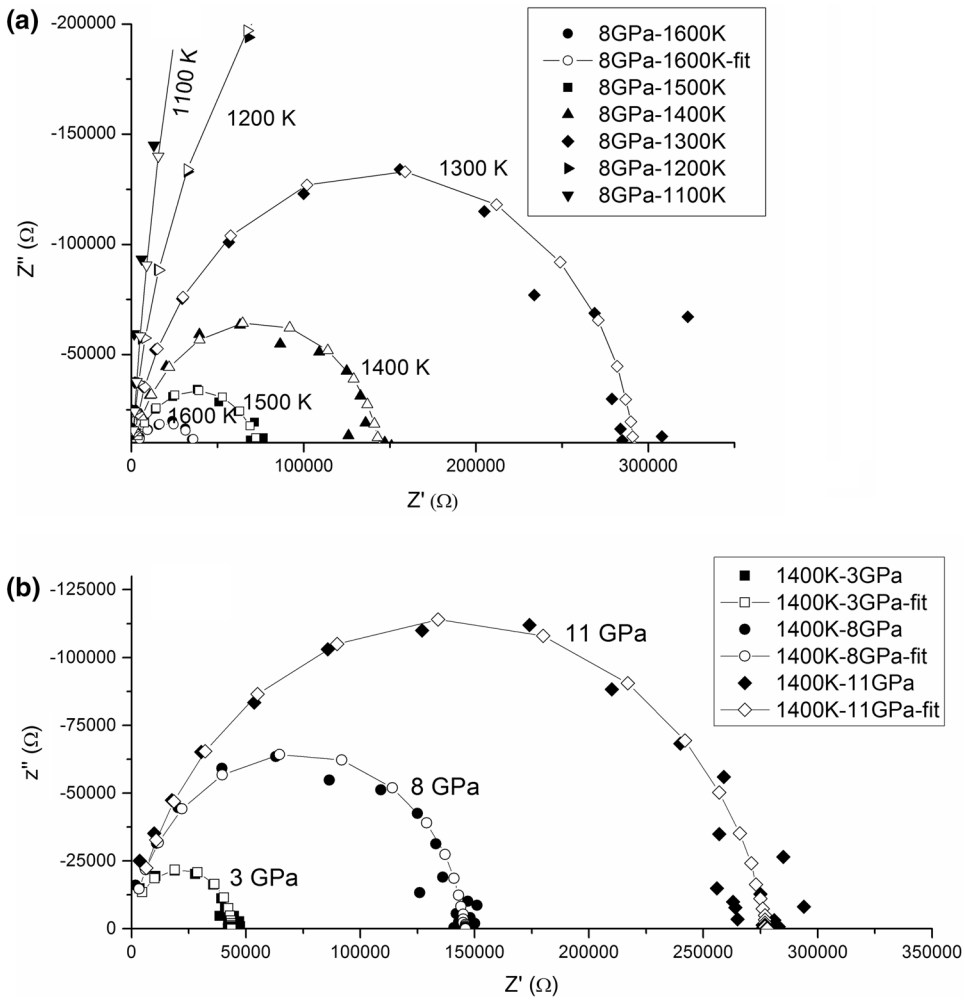

Fig. 4 Representative impedance spectra acquired for R623. **a** Temperature dependence of impedance spectra at 8 GPa. **b** Pressure dependence of impedance spectra from 3 to 11 GPa at 1400 K

Na content at constant temperature (Hu et al. 2013). Therefore, the differences between the results of this study, and those obtained by Hu et al. (2013) and Guo et al. (2015), can be satisfactorily explained by differences in the composition of the starting materials if the small effect of pressure is ignored. The detailed experimental conditions and results are summarized in Table 2.

While the first-principle calculations had predicted that liebermannite with some K^+ vacancies in the crystal structure would be a superionic conductor along the [001] direction (He et al. 2016), we did not observe the high-conductivity behavior of liebermannite polycrystals at high pressure and temperature in this study. The compositional analysis of the recovered sample (Table 1) showed that the concentration of K^+ vacancy, $c(v_{K^+}) = 100 \times \left(1 - \left[K^+\right] - \left[Na^+\right] - \left[Ca^{2+}\right] - \left[Mg^{2+}\right] - \left[Fe^{2+}\right]\right)\%$, was around 35%. However, the electrical conductivity values of liebermannite in this study were four orders of magnitude lower than those reported by He et al. (2016) with 25% K^+ vacancies. According to the theoretical calculation and experimental results, we can conclude that liebermannite is highly anisotropic in terms of electrical conductivity. The conductivity along one crystallographic orientation was at least 10,000 times lower than that along the [001] direction. Extreme anisotropic behavior in terms of electrical conductivity has never been encountered for silicates at high pressures and temperatures in experiments, to the best of the authors' knowledge. The maximum electrical conductivity-related anisotropies for dry or hydrous olivine (Yoshino et al. 2006; Poe et al. 2010; Yang et al. 2012; Dai and Karato 2014), clinopyroxene (Yang et al. 2012), orthopyroxene (Dai and Karato 2009), and plagioclase (Yang et al. 2012) are all lower than 2. In case of hydrous minerals with a layered structure, currently available experimental data indicate that the maximum electrical conductivity-related anisotropies were smaller than 1 (brucite, see Guo and Yoshino 2014; serpentine and talc, see Guo et al. 2011).

Observations of the texture of the recovered sample show that sanidine transformed into a mixture of wadeite-type $K_2Si_4O_9$, kyanite, and coesite at 8 GPa and 1573 K (Fig. 1b). When the sample was further compressed to 11 GPa, the mixture of wadeite-type $K_2Si_4O_9$, kyanite, and coesite was

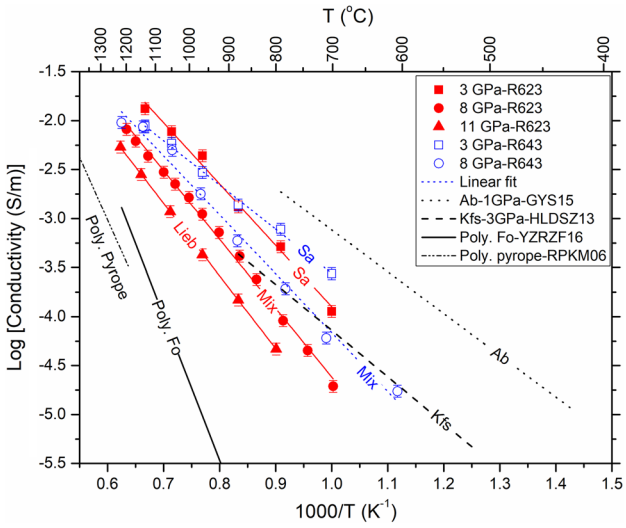

Fig. 5 Electrical conductivity of natural sanidine as a function of reciprocal temperature at 3 GPa, 8 GPa, and 11 GPa, and the comparison between this study and the results reported by Hu et al. (2013) and Guo et al. (2015). Note: HLDSZ13, Hu et al. (2013); GYS15, Guo et al. (2015); YZRZF16, Yoshino et al. (2016); RPKM06, Romano et al. (2006). Errors were estimated to be around 7% in conductivity

transformed into liebermannite, and albite in the starting material transformed into jadeite and stishovite (Fig. 1c). At both 8 GPa and 11 GPa, two thin reaction rims (thinner than 50 µm), consisting of forsterite and pyrope, were clearly identified due to the reactions between the sample and the capsule of MgO (Fig. 1d). The reactions can be described as follows:

$$2KAlSi_3O_8 = K_2Si_4O_9 + Al_2SiO_5 + SiO_2, \quad (2)$$

$$SiO_2 + 2MgO = Mg_2SiO_4, \quad (3)$$

$$3Mg_2SiO_4 + 2Al_2SiO_5 + SiO_2 = 2Mg_3Al_2Si_3O_{12}, \quad (4)$$

The reaction products are unlikely to influence the bulk conductivity seriously, because the conductivities of both garnet and forsterite (Fig. 5) are very low (Yoshino et al. 2016; Romano et al. 2006). It is challenging to assess the quality of the theoretical calculations reported by He et al. (2016) owing to a lack of experimental data on the conductivity and diffusivity of potassium. In practice, the calibration of electrical conductivity through the Nernst–Einstein equation and diffusivity data must be treated with caution because not all electric charge carriers can contribute to conductivity, as shown by Guo and Yoshino (2014), and Guo et al. (2013). According to their data on the conductivity and diffusivity of single-crystal brucite, the ratio of the activated electric charge carriers that can contribute to conductivity is at most 33%. Therefore, the conductivity of liebermannite calculated by He et al. (2016) might have been overestimated by several times.

A considerable amount of evidence supports the claim liebermannite can exist and accumulate within a stagnant slab at the depth of the transition zone. (1) The K_2O concentration of the drilled samples in the oceans was as high as 8.1 wt% in alkali basalts, which could provide enough K to form large amounts of K-hollandite during the subduction process. (2) K-hollandite was one of the run products of hydrated average upper continental crust, MORB, andesite, and pelite at pressures higher than 8 GPa. (3) The stagnation of Pacific plate in the transition zone beneath NE China and the Philippine Sea could provide from time to space to the formation and accumulation of K-hollandite in the transition zone. (4) The folded oceanic crystal layer in the transition zone during subduction process could increase the content of K-hollandite in the transition zone (see the summaries by He et al. 2016). Furthermore, a preferred orientation of [001] for liebermannite is likely to prevail in the stagnant slab beneath NE China and the Philippine Sea owing to the strong shear stress caused by the subducting process and convection at the mantle. An initial purpose of this study was to examine whether the

Table 2 Experimental conditions and results

Run no	Pressure (GPa)	Temperature (K)	Logσ_0 (S/m)	ΔH (eV)	Phase
R623	3	1000–1500	2.36 (20)	1.24 (5)	Sa
	8	1000–1575	2.41 (10)	1.39 (3)	Wa-Ky-Coe
	11	1110–1605	2.34 (2)	1.47 (1)	Ho
R643	3	1000–1500	0.95 (9)	0.90 (2)	Sa
	8	900–1600	1.85 (20)	1.19 (5)	Wa-Ky-Coe
R861	8	1473			Wa-Ky-Coe
K-feldspar[a]	3	873–1173	4.00 (7)	1.02 (2)	Sa
Albite[b]	1	700–1100	1.15	0.85	Ab

[a]Data from Hu et al. (2013). The chemical composition of K-feldspar is $K_{0.95}Na_{0.01}Cr_{0.01}AlSi_3O_8$

[b]Data from Guo et al. (2015). Albite is free of K

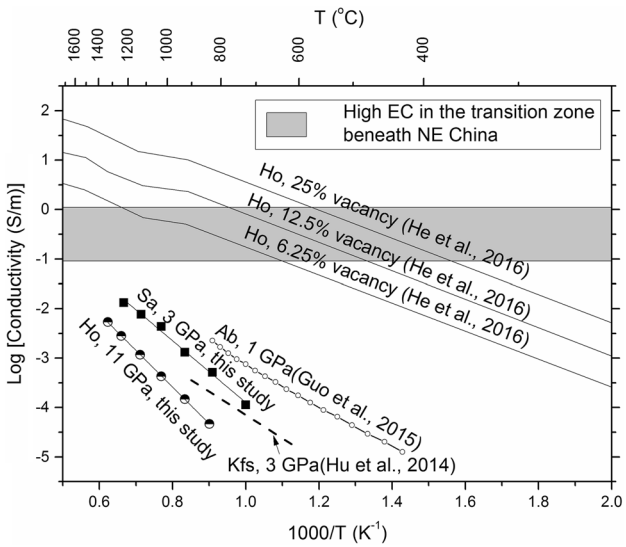

Fig. 6 Comparison between the electrical conductivity of liebermannite in this study, theoretical calculation, and high-conductivity anomalies observed in the transition zone beneath NE China and the Philippine Sea. *Lieb* liebermannite, *Ab* albite, *Sa* sanidine, *Kfs* K-feldspar

electrical conductivity of polycrystalline liebermannite with high K^+ vacancies is high enough to explain the geophysical observations, given that the crystallographic orientation of liebermannite is random distributed. Figure 6 shows the comparison between the electrical conductivity of liebermannite and the high-conductivity anomalies. It is clear that the electrical conductivities of polycrystalline liebermannite (35% vacancies in the K position) in the absence of the preferred lattice orientation along the [001] direction were well below the values obtained through geophysical observations and theoretical calculations. If the theoretical calculations by He et al. (2016) are correct—that is, if liebermannite does exhibit extremely high conductivity-related anisotropy—the preferred orientation of liebermannite along the [001] direction is a necessary condition to explain high-conductivity anomalies. Further measurements of electrical conductivity on single-crystal liebermannite or polycrystalline liebermannite under strong shear deformation should be investigated even though this is challenging to accomplish with the currently available high-pressure technology.

Acknowledgements This study was supported by the National Natural Science Foundation of China (41590623), the National Key Research and Development Project of China (Project 2016YFC0600309), and CAS "Light of West China" program (Y9CR026000 to XG). We thank Shuiyuan Yang for his help in EPMA analysis and Baohua Zhang for valuable comments.

References

Akaogi M, Kamii N, Kishi A, Kojitani H (2004) Calorimetric study on high-pressure transitions in $KAlSi_3O_8$. Phys Chem Miner 31:85–91

Chang L, Chen Z, Liu X, Wang H (2013) Expansivity and compressibility of wadeite-type $K_2Si_4O_9$ determined by insitu high T/P experiments, and their implication. Phys Chem Minerals 40:29–40

Chen S, Guo X, Yoshino T, Jin Z, Li P (2018) Dehydration of phengite inferred by electrical conductivity measurements: Implication for the high conductivity anomalies relevant to the subduction zone. Geology 46:11–14

Chen T, Gwanmesia GD, Ehm L, Losq CL, Reuville DR, Phillips BL, Li B, Liebermann RC (2019) Synthesis and characterization of polycrystalline $KAlSi_3O_8$ hollandite [liebermannite]: sound velocities vs. pressure to 13 GPa at room temperature. CR Geosci 351:113–120

Dai L, Karato SI (2009) Electrical conductivity of orthopyroxene: implications for the water content of the asthenosphere. Proc Jpn Acad Ser B 85:466–475

Dai L, Karato SI (2014) High and highly anisotropic electrical conductivity of the asthenosphere due to hydrogen diffusion in olivine. Earth Planet Sci Lett 408:78–86

Guo X, Yoshino T (2014) Pressure-induced enhancement of proton conduction in brucite. Geophys Res Lett. https://doi.org/10.1002/2013GL058627

Guo X, Yoshino T, Katayama I (2011) Electrical conductivity anisotropy of deformed talc rocks and serpentinites at 3 GPa. Phys Earth Planet Inter 188:69–81

Guo X, Yoshino T, Okuchi T, Tomioka N (2013) H–D interdiffusion in brucite at pressures up to 15 GPa. Am Miner 98:1919–1929

Guo X, Yoshino T, Shimojuku A (2015) Electrical conductivity of albite-(quartz)-water and albite–water–NaCl systems and its implication to the high conductivity anomalies in the continental crust. Earth Planet Sci Lett 412:1–9

He Y, Sun Y, Lu X, Li J, Li H (2016) First-principles prediction of fast migration channels of potassium ions in $KAlSi_3O_8$ hollandite: implications for high conductivity anomalies in subduction zones. Geophys Res Lett 43:6228–6233

Hu H, Li H, Dai L, Shan S, Zhu C (2013) Electrical conductivity of alkali feldspar solid solutions at high temperatures and high pressures. Phys Chem Minerals 40:51–62

Irifune T, Ringwood AE, Hibberson WO (1994) Subduction of continental crustal crust and terrigenous and pelagic sediments: an experimental study. Earth Planet Sci Lett 126:351–368

Khanna SK, Gruner G, Orbach R, Beyeler HU (1981) Thermally activated microwave conductivity in the superionic conductor hollandite ($K_{1.54}Mg_{0.77}Ti_{7.23}O_{16}$). Phys Rev Lett 47:255–257

Langenhorst F, Poirier JP (2000) 'Eclogitic' minerals in a shocked basaltic meteorite. Earth Planet Sci Lett 176:259–265

Le Bas MJ, Le Maitre RW, Streckeisen A, Zanettin B (1986) A chemical classification of volcanic rocks based on the total alkali-silica diagram. J Petrol 27:745–750

Liu X (2006) Phase relations in the system $KAlSi_3O_8$–$NaAlSi_3O_8$ at high pressure-high temperature conditions and their implication for the petrogenesis of lingunite. Earth Planet Sci Lett 246:317–325

Ma C, Tschauner O, Beckett JR, Rossman GR, Prescher C, Prakapenke VB, Bechtel HA, McDowell A (2018) Liebermannite, $KAlSi_3O_8$, a new shock-metamorphic, high-pressure mineral from the Zagami Martian meteorite. Meteorit Planet Sci 53:50–61

Nishiyama N, Rapp RP, Irifune T, Sanehira T, Yamazaki D, Funakoshi K (2005) Stability and P–V–T equation of state of

$KAlSi_3O_8$-hollandite determined by in situ X-ray observations and implications for dynamics of subducted continental crust material. Phys Chem Miner 32:627–637

Poe BT, Romano C, Nestola F, Nestola F, Smyth JR (2010) Electrical conductivity anisotropy of dry and hydrous olivine at 8 GPa. Phys Earth Planet Inter 181:103–111

Romano C, Poe BT, Kreidie N, McCammon CA (2006) Electrical conductivities of pyrope-almandine garnets up to 19 GPa and 1700 ℃. Am Mineral 91:1371–1377

Sueda Y, Irifune T, Nishiyama N, Rapp RP, Ferroir T, Onozawa T, Yagi T, Merkel S, Miyajima N, Funakoshi KI (2004) A new high-pressure form of $KAlSi_3O_8$ under lower mantle conditions. Geophys Res Lett 31:L23612

Urakawa S, Kondo T, Igawa N, Shimomura O, Ohno H (1994) Synchrotron radiation study on the high-pressure and high-temperature phase relations of $KAlSi_3O_8$. Phys Chem Miner 21:387–391

Yagi A, Suzuki T, Akaogi M (1994) High pressure transitions in the system $KAlSi_3O_8$–$NaAlSi_3O_8$. Phys Chem Miner 21:12–17

Yamada H, Matsui Y, Ito E (1984) Crystal-chemical characterization of $KAlSi_3O_8$ with the hollandite structure. Miner J 12:29–34

Yang X (2012) Orientation-related electrical conductivity of hydrous olivine, clinopyroxene and plagioclase and implications for the structure of the lower continental crust and uppermost mantle. Earth Planet Sci Lett 317–318:241–250

Yoshino T, Matsuzaki T, Yamashita S, Katsura T (2006) Hydrous olivine unable to account for conductivity anomaly at the top of the asthenosphere. Nature 443:973–976

Yoshino T, Zhang B, Rhymer B, Zhao C, Fei H (2016) Pressure dependence of electrical conductivity in forsterite. J Geophys Res 122:158–171. https://doi.org/10.1002/2016JB013555